Available online at www.sciencedirect.com
ScienceDirect
International Journal of Heat and Fluid Flow 28 (2007) 575–586
International Journal of HEAT AND FLUID FLOW
www.elsevier.com/locate/ijhff

Unsteady phenomena in the edge tone

G. Paál *, I. Vaik

Department of Hydrodynamic Systems, Budapest University of Technology and Economics, 1521 Budapest, P.O. Box 91, Hungary

Received 21 November 2006; received in revised form 2 April 2007; accepted 19 April 2007
Available online 4 June 2007

Abstract

Despite its geometrical simplicity, the edge tone displays a remarkably complex behaviour. A plane jet oscillates around the wedge-shaped object with a relatively stable frequency and under certain circumstances emits an audible tone. This configuration plays a central role in the sound production of several wind instruments but occurs in industrial situations too. The flow exhibits various interesting nonlinear phenomena reported in the literature which are not entirely explained. In this paper, detailed high precision numerical simulations of the flow are reported under various conditions. Several phenomena are reproduced in agreement with the literature such as the existence of ''stages'', the dependence of oscillation frequency on the outflow velocity and the orifice–edge distance within one stage, the pressure distribution on the edge surface, etc. A criterion for the appropriate time step for constant accuracy has been derived. The location of force action is surprisingly stable; it remains in a very narrow region of the wedge surface independently of the Reynolds number and the orifice–edge distance but it is much further behind the edge tip than reported in the literature. The various stages can coexist in different ways: jumping back and forth between stages or being superposed on each other. Regardless of the form, the first stage continues to be dominant even when the second and third stage appears. The question of disturbance propagation velocity and disturbance wavelength is also investigated. The development of higher harmonics of a single stage along the orifice–edge tip distance is presented.

Keywords: Edge tone; Oscillating flow; CFD; Stages; Acoustic dipole

1. Introduction

The edge tone has been the subject of intensive research for over one and a half centuries. For a review see for example Rockwell and Naudascher (1979). The configuration consists of a plane jet, and a wedge-shaped object placed roughly opposite to the jet exit, traditionally called the edge (Fig. 1). Despite its simplicity, the configuration displays a remarkably complex behaviour. The jet oscillates around the edge with a stable frequency and under certain circumstances emits an audible tone. The configuration is thought to be the central element of some wind instruments. Other practical examples include the tongue of the spiral casing in radial turbomachines and Y-shaped pipe branches. For our purposes, in addition, it plays the role of a model aeroacoustic system in which we can demonstrate that our algorithm for flow-induced sound simulation works properly. The latter work will be presented elsewhere.

The formation of the oscillation is attributed to a feedback loop (Powell, 1961): the oscillating jet creates a dipole-type sound source on the wedge which initiates infinitesimal disturbances at the jet exit – at low Mach numbers with zero time delay. The disturbances grow streamwise along the jet, providing the oscillating jet motion and thus the oscillating force on the wedge surface for the formation of the dipole. If either of v or h is changed continuously, the frequency changes continuously within a certain range but then at certain values the frequency suddenly jumps to another value and the qualitative appearance of the flow also changes. These continuous regions are called ''stages'' or ''hydrodynamic modes''. Fig. 2a, b

* Corresponding author. Tel.: +36 1 463 2991; fax: +36 1 463 3091.
E-mail address: paal@hds.bme.hu (G. Paál).

0142-727X/$ - see front matter © 2007 Elsevier Inc. All rights reserved.
doi:10.1016/j.ijheatfluidflow.2007.04.011

Nomenclature

A	velocity amplitude in Eq. (3) (m/s)
C	constant in Eq. (1) (m^{n-1})
e	accumulated error from temporal discretisation (m/s)
F	force acting on the wedge (N)
f	frequency (Hz)
Δf	frequency resolution of spectra (Hz)
$H1$	length of the nozzle (mm)
$H2$	length of the wedge (mm)
h	nozzle–wedge distance (mm)
M	torque (Nmm)
N	stage number in Eq. (2), number of time steps in Eq. (3) (–)
n	exponent in Eq. (1) (–)
Re	Reynolds number (–)
St	Strouhal number (–)
T	total duration of simulation (s)
u_d	disturbance propagation velocity (m/s)
$V1$	notation in Fig. 2 (mm)
$V2$	notation in Fig. 2 (mm)
v	mean inlet velocity (m/s)
x_F	distance of the point of force action from the edge tip (mm)
α	angle of the wedge (°)
δ	width of the slit of the nozzle (mm)
ε	fractional number in Eq. (2) (–)
λ	wavelength of the disturbance (mm)
μ	dynamic viscosity of air@25 °C (kg/ms)
ν	kinematic viscosity of air@25 °C (m^2/s)
ρ	density of air@25 °C (kg/m^3)
τ	time step (s)

Subscripts and superscripts

x, y, z	length coordinates
rms	root mean square

and c shows the qualitative appearance of the flow in the 1st, 2nd and 3rd stages, respectively. Electronic annex is attached to this paper; there spectacular animations show the various stages in motion.

The oscillation frequency depends on two primary factors, the jet–edge distance, h, and the mean exit velocity v. The system behaviour is also influenced by a number of secondary factors, such as the exit velocity profile, the shape of the nozzle, the sharpness and the transversal position of the edge, etc. (Ségoufin et al., 2004). The edge angle, however, was found to play no role under 40°. The basic relationship between the frequency f and the above-mentioned parameters is:

$$f = C\frac{v}{h^n} \tag{1}$$

where C is a constant. (In some papers, there are additive constants to v or to h but we are concerned here with the general trends.) About the value of the exponent n there has been a long debate. In the early phase of the research rather $n = 1$ was favoured, (Brown, 1937) later it became generally accepted that $n = 3/2$ (Curle, 1953; Holger et al., 1977; Crighton, 1992). Jones (1942) found a variety of exponents, all between 1 and 3/2, depending on the stage number. Recent research (Bamberger et al., 2004) and also the present paper indicate that $n = 1$ is more correct.

Some authors report (e.g. Brown, 1937; Nyborg et al., 1952; Powell, 1961) about a hysteresis phenomenon, meaning that the jump from one stage to another takes place at another value when increasing the parameter, than when decreasing it. Other authors do not find such a phenomenon. The existence of stages is explained by the fact that between the jet exit and the edge a certain phase relationship must be maintained. Within a parameter region this can be achieved by adjusting the frequency by keeping the wavelength approximately constant, over a certain value, however, the wavelength must be adjusted to a completely different value. The phase relationship is summarized in the following equation:

$$h = \lambda(N + \varepsilon) \tag{2}$$

where λ is the wavelength of the disturbance, N is a whole number corresponding to the stage number, ε is a small number indicating that the effective resonance length of the edge tone system is somewhat longer than h, or in other words the effective point of action of the pressure-induced force on the edge is $\varepsilon\lambda$ distance away from the tip. There is no agreement in the literature about the value of ε, it may also depend on the details of the configuration and on stage number. The most often occurring value is 1/4 (Curle, 1953). The wavelength can be determined from the frequency of oscillation and the phase speed of the disturbance. As we shall see later in the paper there are some basic difficulties with this concept.

Almost all the authors of experimental studies worked with fully developed parabolic jet exit velocity profiles. Exceptions are Krothapalli and Horne (1984) who found that the top hat exit velocity profile allows the coexistence

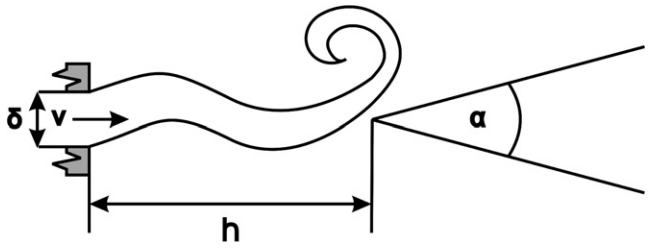

Fig. 1. Basic configuration of the edge tone.

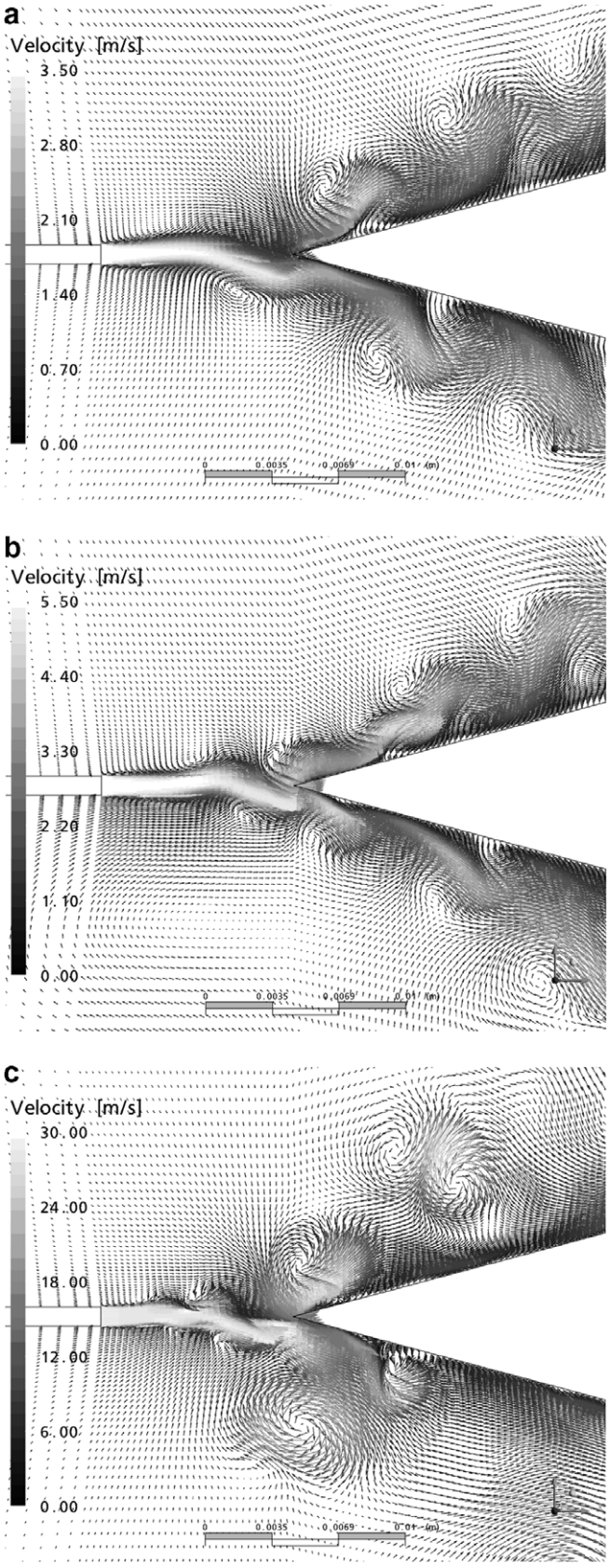

Fig. 2. Qualitative appearance of the stages; for all figures $h/\delta = 10$; (a) stage I $Re = 225$; (b) stage II $Re = 350$; (c) stage III $Re = 1800$.

of several stages at the same time and Ségoufin et al. (2004) reporting that the oscillation frequencies with a top hat profile rose by a factor of 1.5 compared to the parabolic profile.

The first goal of this paper was to reproduce certain features of the edge tone system known from experimental work (Brown, 1937; Jones, 1942; Nyborg et al., 1952; Powell, 1961; Kaykayoglu and Rockwell, 1986a,b) and from theoretical considerations (Curle, 1953; Holger et al., 1977; Crighton, 1992) on the basis of detailed and accurate direct numerical simulations. These include the existence of and quantitative evaluation of stages, the determination of disturbance propagation velocity, the pressure distribution on the wedge surface, the point of force action, etc. There are two papers known to the authors where numerical simulations on the edge tone are described (Ohring, 1986 and Bamberger et al., 2004) but the present work covers a much wider range of parameters and reaches broader conclusions.

It has to be mentioned that Howe (1975) used a different approach to a related problem. He applied his reformulation of Lighthill's aeroacoustic theory among other examples to the theory of the flute. The sound production of the flute profits from the edge tone oscillation but the oscillation transforms under the presence of the resonator. He calculated vortex sound sources generated by the edge tone using a simplified model.

The paper is structured as follows. First the numerical method for the flow simulation is described. After a satisfactory level of confidence in the methodology is gained, the simulation can be used as a tool to perform parametric studies and to gain new physical insights into the fluid mechanics of the edge tone.

2. Numerical procedures

2.1. Flow simulation

2.1.1. Flow domain and computational mesh

The geometry and the mesh were generated with the software ANSYS ICEM.

The domain of the simulation can be seen in Fig. 3. The geometrical measures are the following: $V1 = V2 = H2 = 75$ mm; $H1 = 12.5$ mm; $\alpha = 30°$; $\delta = 1$ mm. The distance h is varied in the paper; the values will be given later.

The velocity profile was top hat; the jet exit was sharp edged. Preliminary results indicate that the exit velocity profile strongly influences the oscillation but the results with the parabolic profile will be published later. The flow was assumed to be two-dimensional, and since the software used is three-dimensional, a one cell thick layer was used for the simulations. The assumption is justified: all the experimental studies used a high aspect ratio nozzle and edge and no three-dimensional effects have been found. A three-dimensional simulation was also performed and in the central region the flow proved to be almost perfectly two-dimensional.

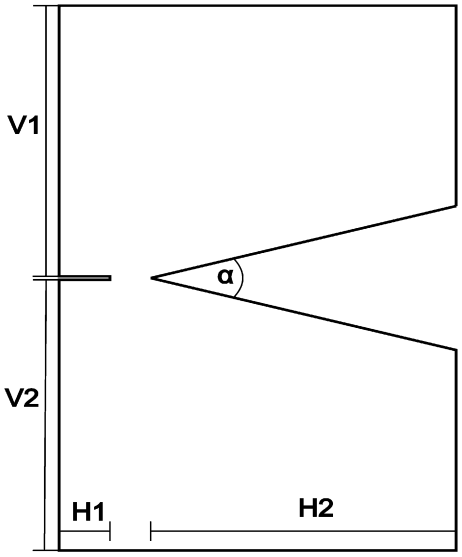

Fig. 3. Solution domain.

The boundaries were far enough from the region of interest not to have a disturbing effect on the flow. Our experience showed that it is advantageous for the flow development if the back boundary is placed somewhat behind the nozzle exit ($H1$); otherwise unphysical vortices might appear in the flow.

In order to increase the simulation accuracy a block-structured hexagonal mesh was used (Fig. 4). Extensive mesh convergence studies have been performed in one geometry ($h = 10$ mm and $Re = \delta u/v = 200$) and in this case the mesh finally used contained 36,300 hexahedral elements. Coarser meshes were not satisfactory because certain important flow structures were not well resolved and finer meshes were not necessary because the result changed only negligibly, while the run time increased dramatically. Increasing the number of cells by a factor of 2.4 the frequency peaks remained exactly the same and the force acting on the edge changed less than 2%.

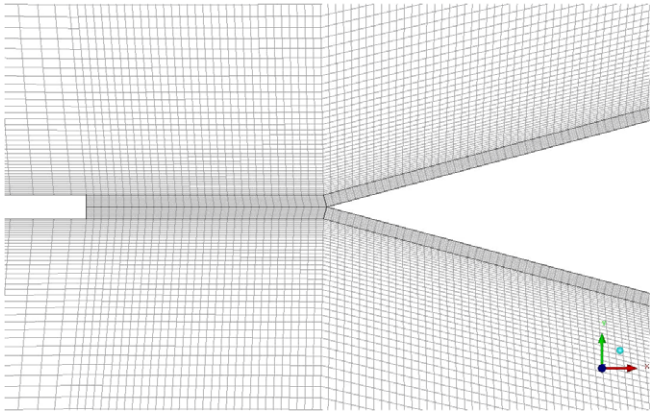

Fig. 4. Detail of the mesh with block boundaries, $h/\delta = 10$.

Here the nozzle exit-wedge tip distance was covered by 32 elements. When the distance h was varied, the number of elements in this region was increased proportionally.

2.1.2. Boundary conditions, flow and simulation parameters

On the two planes bordering the 2D slice symmetry boundary conditions were prescribed. At the solid walls of the wedge no slip boundary conditions whereas at the outer nozzle wall free slip conditions were given. At the back wall a small (about 1% of the exit velocity) inflow was prescribed. This was done in order to stabilize the flow, while not influencing the parameters studied. The spectral peaks appear at the same frequencies but they get sharper. Without this, experience shows that there is an increased risk that non-physical vortices appear and remain in the domain. As mentioned before, at the nozzle exit uniform velocity distribution was assumed. All other boundaries were set to opening boundary condition, i.e., prescribed static pressure with no prescribed flow direction.

Air at 25 °C ($\rho = 1.185$ kg/m^3, $\mu = 1.831 \times 10^{-5}$ kg/ms) was used as the fluid. The flow was assumed to be incompressible and laminar, so that no turbulence model was needed. Second order accurate spatial and temporal discretisations were used.

It has been tested to what extent the initial condition influences the result. To this end simulations with initially quiescent fluid and initially steady state flow have been performed. It turned out that the initial condition has no influence on the final character of the flow. No special measures had to be taken to initiate the oscillation; the oscillation set in spontaneously after a short transient period.

Great care was taken to determine the optimum temporal resolution. First, the optimum time step was determined for a reference case ($Re = 200$, $h/\delta = 10$). For this case simulations with time steps of 0.05, 0.1, 0.2 and 0.4 ms were carried out to determine the optimum time step. After careful comparison of the pressure and velocity time signals and the spectra of these signals at several points it was found that 0.2 ms is a golden mean between computation resources and accuracy. The frequency of the oscillation here is 112 Hz, so this meant about 45 time steps per cycle. After this, an analytical criterion to keep the error of the temporal discretisation constant was derived, resulting in the following equation: the discretisation error remains constant if

$$e^T T \tau^2 A f^3 = \text{const} \tag{3}$$

where τ is the time step, f is the expected oscillation frequency, T is the duration of the simulation and A is the amplitude of the velocity oscillation. The duration of the simulations T (in simulated time) was mainly determined by the required frequency resolution of the spectra ($\Delta f = 1/T$). Of course, with decreasing time step, it becomes increasingly difficult to get the same absolute frequency resolution in a reasonable time. It was decided that the dura-

tion of the simulation should ensure a frequency resolution of 1–2% of the expected maximum frequency. Each simulation included also a transient part in the beginning before the quasi-steady oscillation sets in. This transient part was omitted from the signal when performing FFT. Fortunately it turned out that the duration of the transient part decreased linearly with increasing frequency. That means that the total duration of the simulation could be reduced inversely proportionally with frequency while keeping a constant relative frequency resolution. "A", the velocity oscillation amplitude, on the other hand, increases proportionally with the exit velocity. This leads to the conclusion that, in order to keep the error constant, the time step has to be decreased faster than inversely proportionally with the mean velocity, it has to be proportional with $v^{-3/2}$.

The details of this derivation are given in Appendix A. The number of time steps per cycle increases from about 34 at $Re = 100$ to 272 at $Re = 1800$.

Pressure and velocity histories were written out in several points of the flow field and the frequencies were determined by means of FFT (using MATLAB). No significant differences were found in the frequencies whether velocity or pressure histories were used and whether this or that point was used.

It has to be mentioned that when a simulation is started the expected oscillation frequency and thus the required time step can be estimated by linear extrapolation (Eq. (1)). When a higher stage appears with a sudden frequency rise then the simulation has to be repeated with the time step adjusted accordingly. The memory requirement for these simulations was rather low because of the small mesh, but one simulation typically took two days of CPU time for low Reynolds numbers and up to two weeks for higher Reynolds numbers on an Intel Pentium 4, 3.2 GHz machine because of the large number of time steps.

3. Results and discussion

The first remarkable result is that the existence of three stages has been reproduced by simulation, to the best knowledge of the authors, for the first time. The qualitative pictures of the three modes are displayed in Fig. 2a–c. It is clearly seen that the mode (or stage) order number roughly corresponds to the number of half-waves between jet exit and wedge. The periodic vortex shedding can be very nicely observed in these figures.

Two kinds of systematic parameter studies were performed:

(i) the h/δ value was kept fixed at 10 and the Reynolds number ($Re = \delta v/\nu$) was varied between 100 and 1800 with larger increments for higher Re values. (The Reynolds number was changed by changing the exit velocity);
(ii) the Reynolds number was kept fixed at 350 and the h/δ value was varied ($h/\delta = 3$, 4, 5, 6.25, 7.5, 8.75, 10 and 15)

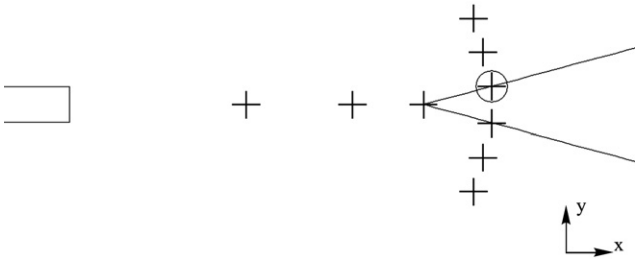

Fig. 5. Monitoring points.

For quantitative analysis of the results several points were defined to obtain pressure and velocity values from. Pressure signals were read out from points from the upper and lower side of the wedge and also from the symmetry axis between the orifice and the wedge. Transversal velocity values were read out only from the symmetry axis in the same points as for the pressure signals (see Fig. 5).

From these signals the dominant frequency components and their amplitudes were calculated with FFT using MatLab and also other parameters determined.

The frequency – as expected – does not really depend on the position of the point. It should be noted that in some – but not in every – simulations the dominant frequency of the pressure signal at the symmetry axis is the twice the oscillation frequency because the pressure is insensitive to the direction of the jet deflection. Hence the oscillation frequency of the jet was calculated from the pressure signals at upper and lower side of the wedge or the transversal velocity signals from the symmetry axis.

3.1. Frequency analysis

In Figs. 6 and 7, the frequency and the Strouhal number ($St = f\delta/v$) is presented as a function of the Reynolds number, respectively. The error bars in the figures represent the width of the spectral peak. In many of the points the error bars cannot be seen because of the size of the markers.

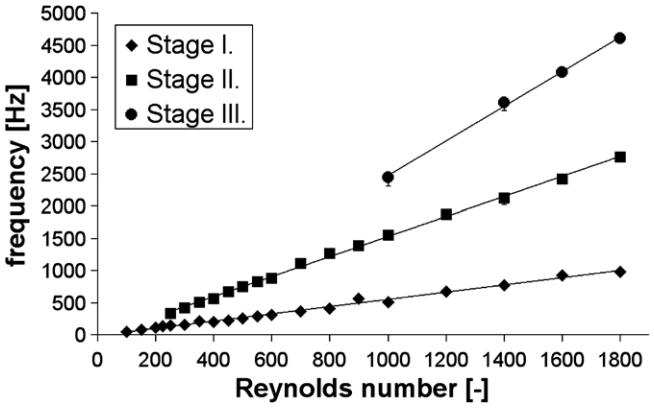

Fig. 6. Frequency as a function of Reynolds number.

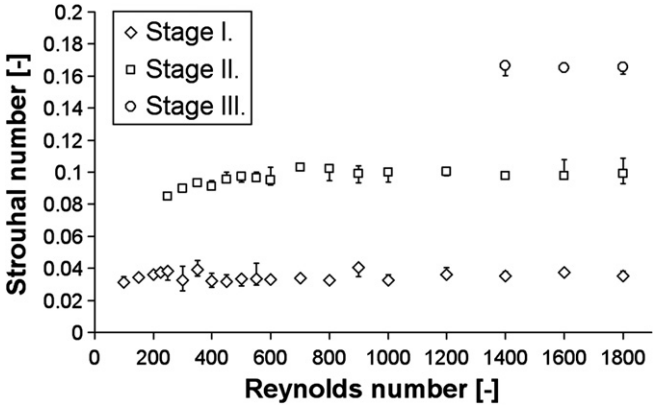

Fig. 7. Strouhal number as a function of Reynolds number.

Agreeing well with the literature (e.g. Powell, 1961), it can be seen, that the frequency is a linear function of the Reynolds number within one stage but with different slopes in different stages, and the Strouhal number is nearly constant in each stage. The deviation of the Strouhal number from constancy, with the exception of the very beginning, is within the uncertainty of the frequency reading. That is determined by the frequency resolution of the spectrum and the width of the spectral peak and stays always within 10% of the peak frequency. One big difference relative to Powell's findings is that when the Reynolds number is increased the first stage does not disappear here but coexists further with the higher stages. Preliminary results with parabolic inlet profile and also the literature indicate that this difference is related to the difference between the inlet profiles. The coexistence of the stages can take place in different ways. At lower Reynolds numbers there is a random jumping from one pure stage to the other or even more often, the lower stage is pure, the higher stage is a superposition of the two signals. At higher Reynolds numbers the various stages are superposed to each other without jumping. When two or three stages are superposed (which are not harmonically related to each other), the motion becomes very complicated and is not periodic. Examples for the two kinds of behaviour are shown in Figs. 8a and 8b.

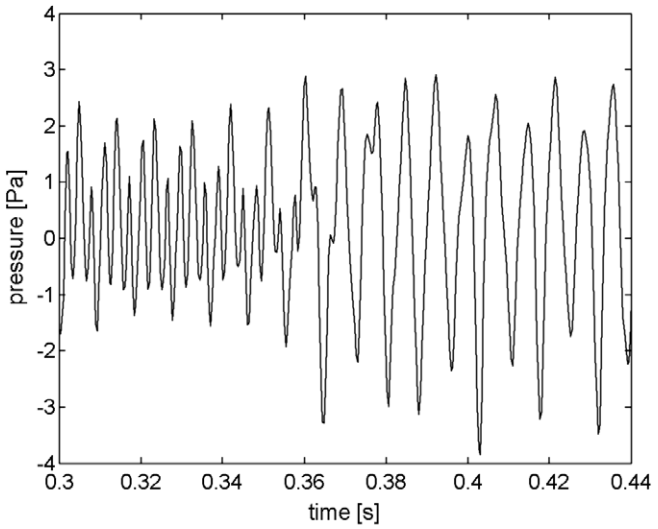

Fig. 8a. Time history of the pressure in a point on the edge surface for $Re = 250$.

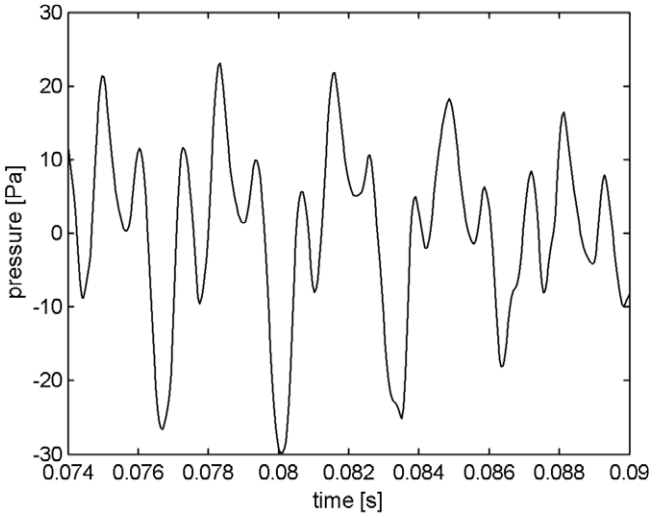

Fig. 8b. Time history of the pressure in a point on the edge surface for $Re = 600$.

For the investigation of the h-dependence the Reynolds number was kept constant at 350. For $h/\delta = 3$ there was no edge tone activity, the flow remained steady. The first stage of the edge tone appeared at $h/\delta = 4$ and till $h/\delta = 7.5$ only the first stage was present. From $h/\delta = 7.5$ the second mode appeared but the first mode was still present. For the $h/\delta = 15$ case only the second mode evolved.

From the results of the simulations with $Re = 350$ it was found out that the relationship between the oscillation frequency and the nozzle-wedge distance not the recently generally accepted relationship $f \sim h^{-3/2}$ but $f \sim h^{-1}$. A similar result was reported recently by Bamberger et al. (2004). For both stages, the result was similar (Figs. 9a and 9b). Simulations for other Reynolds numbers confirmed this relationship.

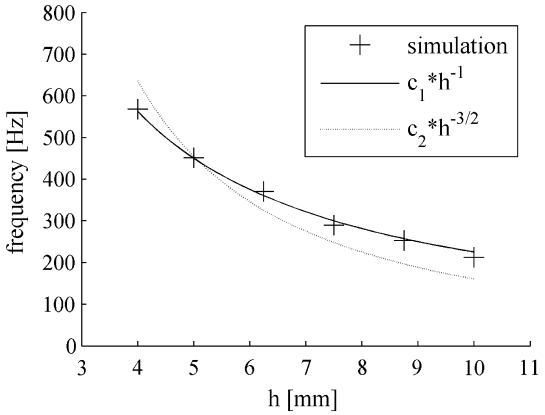

Fig. 9a. h-dependence of the frequency, $Re = 350$, Stage I.

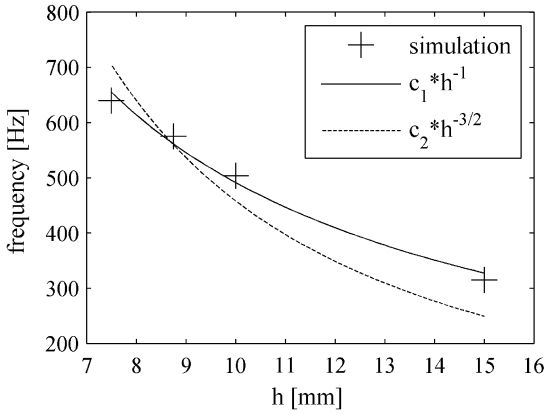

Fig. 9b. h-dependence of the frequency, $Re = 350$, Stage II.

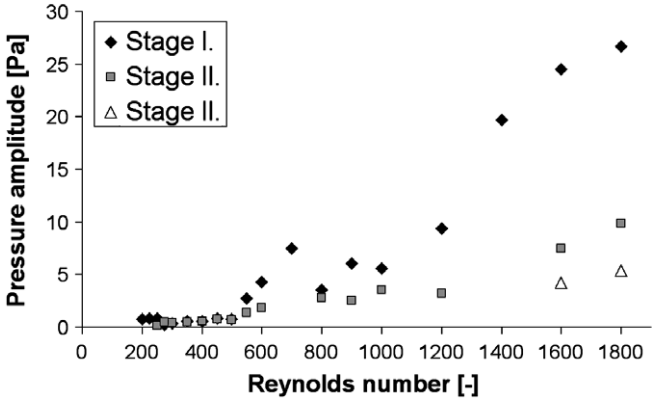

Fig. 10. Amplitude of the various stages in the pressure signal at the point indicated with a circle in Fig. 7.

For comparison a best fit $h^{-3/2}$ curve was included to show to what extent this relationship is incorrect.

In Fig. 10, the amplitude of the various stages is plotted against the Reynolds number. In the range of the investigated Reynolds numbers basically the amplitudes of all stages increase showing no sign that one of the lower stages is bound to disappear. Also, contrary to the expectations, the lower stages continue to dominate at higher Reynolds number. Even higher Reynolds numbers will be investigated whether this trend changes.

3.2. Pressure distribution on the wedge and location of force action

In Fig. 11 the rms pressure distribution along the wedge can be seen. All Reynolds numbers display a similar distribution except for the magnitude of the pressure. The sharp peak in the immediate vicinity of the wedge tip is followed by gradual drop, a second, flatter peak, and finally a slowly decreasing long region. The distribution is basically similar to that of Kaykayoglu and Rockwell (1986a), found experimentally. Kaykayoglou and Rockwell found that after a medium value the pressure reaches a sharp maximum close to the wedge tip and afterwards the pressure decreases roughly as $\sim x^{-1/2}$. They measured the pressure only in a few points. The basic features are reproduced here with the sharp peak close to the edge tip. Since our spatial resolution is higher, more details can be seen in Fig. 11 than in Kaykayoglu and Rockwell (1986a). The distribution can be represented rather with a piecewise linear than with a power function. Another difference is that there the total streamwise length of the wedge was 0.8 h, whereas here much longer, 7.5 h. Since the pressure is non-negligible along almost the whole length of the wedge, the point of force action (x_F) is much more behind the tip in our case than in theirs.

This point has an importance because this point should indicate the effective location of the acoustic dipole.

The mean x_F is calculated as

$$\bar{x}_F = \frac{M_{zrms}}{F_{yrms}} \tag{4}$$

(Both the torque and the force are meant per unit length.) The instantaneous value of x_F is calculated with the instantaneous values of the torque and the force.

For comparison: Kaykayoglou and Rockwell found roughly $\bar{x}_F/h = 1/4$ whereas here it is 1.6–2 measured from the tip. The temporal history of x_F is shown in Fig. 12 and we can see that the point of force action remains in a narrow range most of the cycle. Every half cycle we see singularities that are physically not realistic; they indicate that the y component of the force gets zero twice in a cycle.

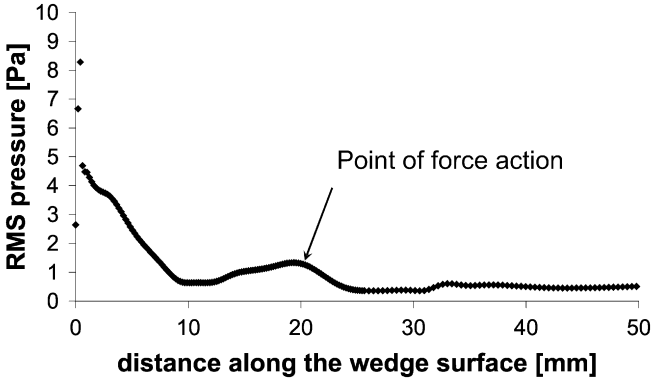

Fig. 11. Pressure distribution along the wedge surface.

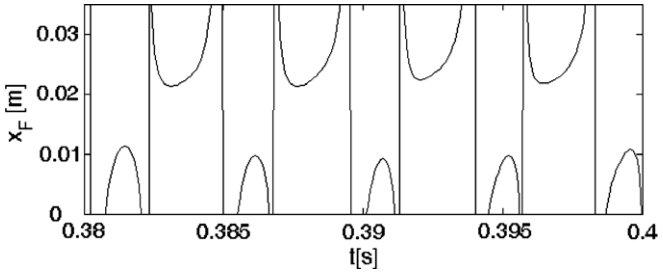

Fig. 12. Point of force action varying in time; $h/\delta = 10$, $Re = 350$.

The location of $\bar{x}_F$ is remarkably stable both as a function of the Reynolds number and of h (lies always between 16 and 20 mm from the tip). That means that the location of the effective sound source is largely independent of the details of the flow as long as the wedge geometry is unchanged. So the dimensionless form of $\bar{x}_F$ is not constant.

If we take a look at the time-resolved distribution of pressure along the wedge surface (not shown here), we see a regular wave pattern running along the wedge over the period but with the same characteristic peak at each instant near the tip.

In Fig. 13, the two components of the force per unit length can be seen as a function of the inlet velocity. The force is calculated by integrating the static pressure over the whole wedge surface. The dependence is perfectly parabolic for both components. This can be explained in the following way. The force is proportional with the dynamic pressure on the surface; this is proportional with the square of the velocity perpendicular to the wedge surface. This again must be proportional with the inlet velocity. This leads to the conclusion that the transversal velocity amplitude averaged in some sense increases proportionally with the inlet velocity.

3.3. Disturbance propagation velocity and wavelength of the disturbance

It is crucial in the understanding of the exact mechanism of the edge tone oscillation to determine the velocity of the disturbance along the jet. In the literature a theoretical value of 0.5 times the mean exit velocity is given (Mattingly and Criminale, 1971). The theory is with an assumption of an inviscid parallel jet and corresponds to the phase velocity of the most unstable frequency disturbance. Experimental values scatter around 0.4 times the mean exit velocity (e.g. Ségoufin et al., 2004). The expression "phase velocity" is meaningful only if there is only one mode present; when several modes are superposed on each other, each mode might propagate with a different velocity or the various modes might interact with each other in an unknown way. If in multimode operation a disturbance propagation velocity can be identified then it is not a phase velocity; or, alternatively the phase velocity can be determined for each mode separately. Here only the single mode case will be considered. The disturbance velocity was determined with three different techniques; two different correlation techniques and one using the phase spectrum from the FFT. There will be later a complete publication dedicated to the question of the disturbance propagation velocity; the techniques will be described there in detail. All three methods give very similar results, the most reliable and simple being the third one so that the results presented here are based on that. The phase for signals of the pressure, the streamwise and the transversal velocity on the jet centreline are presented in Fig. 14 for two different Reynolds numbers. The absolute numbers on the vertical axis are not important; the starting points of the three curves were adjusted in an arbitrary manner to 0, 1 and 2, respectively. The relative phase from the starting point is to be observed. The reciprocal of the derivative in each point multiplied with the angular frequency yields the phase velocity. It is demonstrated in Fig. 14 that these curves are universal in the sense that they apply for every first stage single-mode Reynolds number (It has been tried for many more cases than presented.) The first and the last mms of the curves are cut off; in the first mm the disturbance is not yet enough developed and on the last mm the edge influence is too strong.

In spite of the appearance in the figure the total phase delay of the pressure and the streamwise velocity over the whole distance is the same. The apparent frequency of these two variables is the twice the fundamental since they have no sign. The frequency of the transversal velocity is

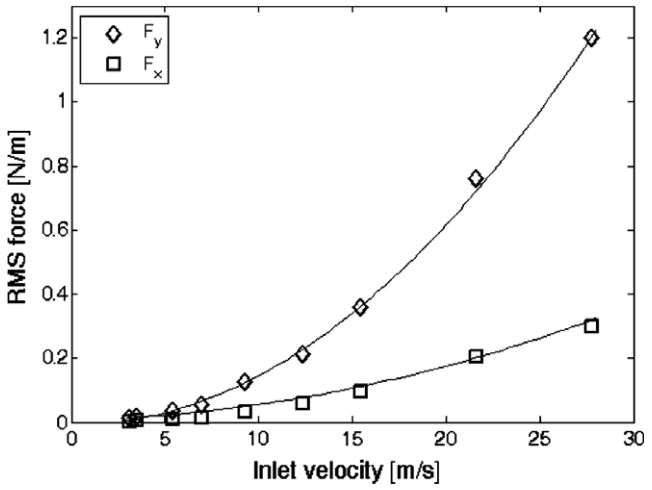

Fig. 13. Force per unit length on the upper wedge surface as a function of inlet velocity; $h/\delta = 10$.

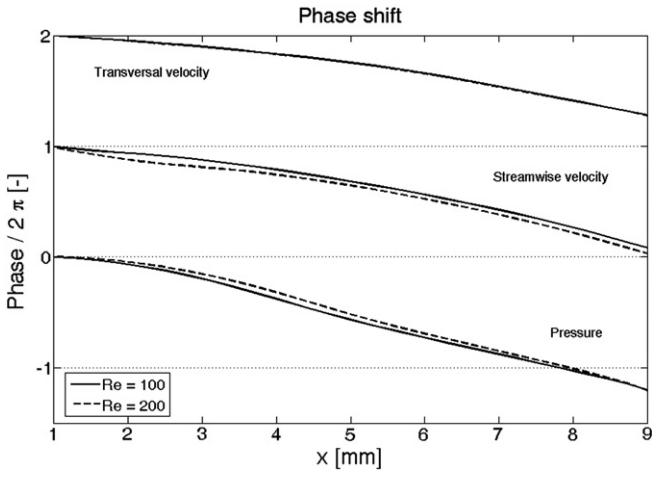

Fig. 14. Relative phase of signals of various variables along the jet axis for two different Reynolds numbers; $h/\delta = 10$; single mode operation.

the fundamental thus total phase delay is expected to be half of that of the previous signals. Instead, it is somewhat more than that and we have no explanation for this. The phase velocities are very high (more than v) at the orifice and they continuously and rapidly decrease further downstream to values of 0.5–0.6v for the transversal velocity signal, and to 0.35–0.5v for the other two signals. This latter agrees well with the value found by Ségoufin et al. (2004) but it is also not far from the theoretical value of Mattingly and Criminale (1971). The initially high velocities can be explained so that the disturbances have not developed there yet – instead the jet moves rather like a "solid stick". Since there is a continuous change of the phase velocity it makes no sense to talk about "wavelength" in the traditional sense of the word since within one wavelength the "wavelength" changes. A further discussion of this subject follows in another publication. Preliminary results for multimode operation show that the propagation velocity of each mode separately stays in this region of 0.35–0.5 v most of the distance.

3.4. Development of higher harmonics

The development of higher harmonics can be analyzed only at lower Reynolds numbers or lower h values. The reason for this is that with increasing Re or h when the higher modes appear their spectral peak becomes increasingly broader and it becomes very difficult to distinguish the higher harmonics of lower modes from higher modes.

Fig. 15 shows the development of the various harmonics at a moderate Reynolds number on the centerline. The shape of the functions is the same for all single-mode Reynolds numbers. In the case of the pressure and the streamwise velocity there is a typical exponential-type rise in the amplitude for all harmonics in the beginning indicating the linear region of disturbance growth and then the saturation region and a decrease. The maximum is for both variables at 8 mm, which is 80% of the orifice–edge tip distance. This remains true also for other h values. The last point at the tip of the edge in the case of the pressure is much higher but that can be considered as a singularity because of the stagnation point at the sharp edge. For these two variables, it is not surprising that the first overtone dominates; neither of these variables can distinguish between up and down because of the symmetry, so that the apparent oscillation frequency is twice the fundamental. The transversal velocity (Fig. 15c) behaves differently. In line with the expectations the dominant mode is the fundamental since here the direction of the motion is resolved. However, the shape of the function is different. There is a linear rise at the beginning, a short constant region and then a much sharper rise in the fundamental and a slight decrease in the higher harmonics. The second harmonic is higher than the first which can again be explained by the symmetry of the geometry. The reason for the sharp rise

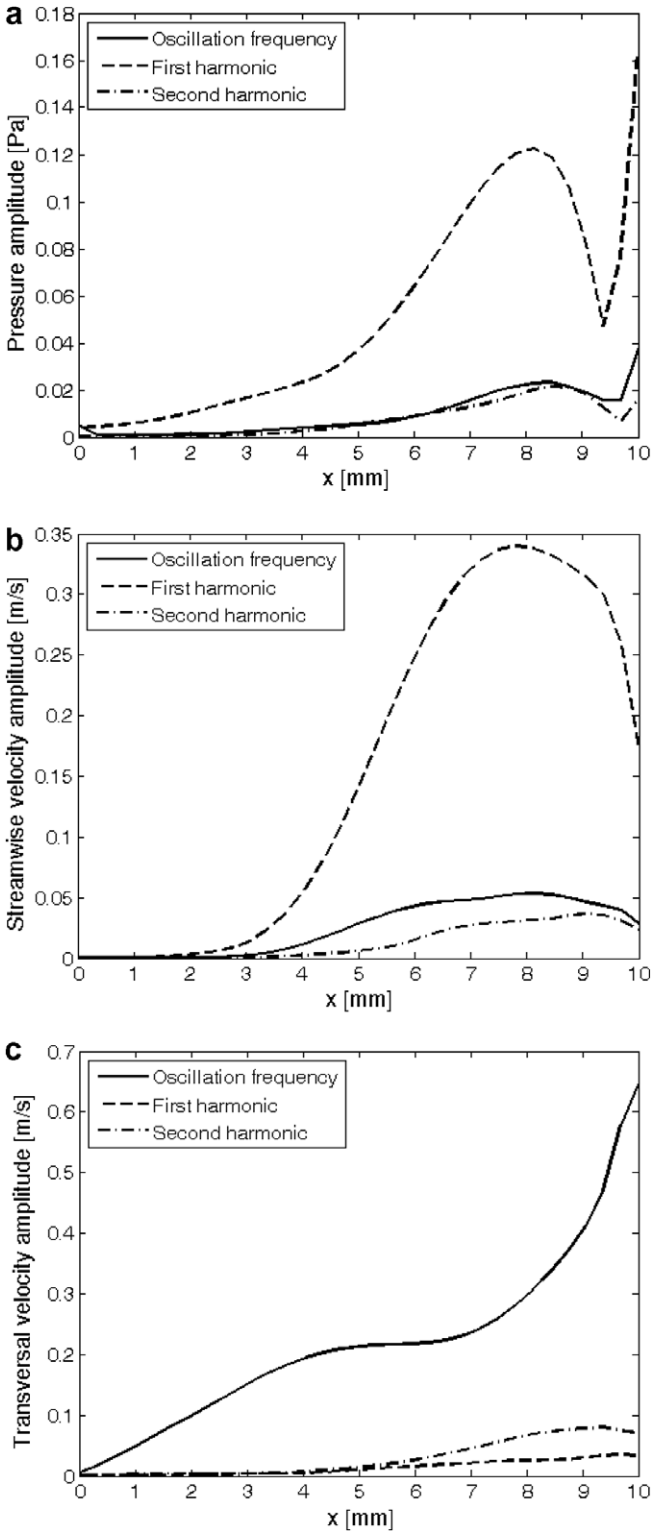

Fig. 15. Development of the higher harmonics along the axial coordinate. $Re = 200$, $h = 10$ mm. (a) pressure; (b) streamwise velocity; (c) transversal velocity.

near the edge is the acceleration of fluid between the vortex near the edge and the edge. We have nevertheless at present no satisfactory explanation why the different variables display a different shape. The shape is no coincidence; it

looks the same for other Reynolds numbers and for other h-s.

4. Conclusions and outlook

Detailed high precision numerical flow simulations have been performed on the edge tone. The existence of the first three stages has been reproduced by numerical simulation for the first time to the best knowledge of the authors. The Reynolds number dependence of the frequencies corresponds to the expectations, whereas the dependence on the jet exit-wedge tip distance was proved to have an exponent of -1 instead of a long-accepted $-3/2$. The lower stages do not disappear at higher Reynolds numbers within the investigated Reynolds number range. The coexistence of different modes takes place by jumping in and out of the lower mode at lower Reynolds numbers and by superposition of the two or three modes at higher Reynolds numbers. Even in the presence of the higher stages the first stage has the highest energy content. The qualitative shape of the pressure distribution along the wedge has proved to be similar to the experimental results of Kaykayoglu and Rockwell (1986) but due to the better resolution and accuracy it has been shown that the point of force action is significantly further behind the wedge tip than stated by them. This location, however, is more or less independent of both the Reynolds number and the nozzle exit-wedge distance. The mean force on the wedge surface increases quadratically with the exit velocity. Phase velocities of the disturbance propagating along the wedge have been determined. In the initial part the phase velocity was high, in the order of the exit velocity, later the velocity slowed down to values of around 0.4 times the exit velocity. The amplitudes of all harmonics showed a characteristic initial exponential rise, saturation, marked by a maximum and a decrease for the pressure and for the streamwise velocity and a different shape for the transversal velocity. Whereas in the former two variables the first harmonic dominates, in the third one the fundamental dominates, easily explainable with symmetry considerations.

Plans in the near future:

- Further parameter studies including detailed simulations with parabolic inlet profile, different nozzle or edge geometry.
- Mapping of the parameter space of the onset of oscillation and the appearance of higher stages.
- Extending the simulations to the turbulent regime.
- A comparative study of the various definitions of the disturbance propagation velocity.
- Theoretical modelling.

Acknowledgements

This work has been supported by the Hungarian National Fund for Science and Research under contract Nr. OTKA T46304. I. Vaik was supported by the System International Foundation.

Appendix A

It is well known that the main source of the error in the numerical solution of a time-dependent partial differential equation is the accumulated error of the discretised time derivatives over many time steps. ANSYS CFX uses the "Second Order Backward Euler" time discretisation scheme. In this Appendix, a conservative estimate for the time discretisation error of this scheme will be given (Stoyan and Takó, 1995).

As a first step, let us analyze this scheme via the numerical solution of an ordinary differential equation (thereby assuming that the error from the spatial derivatives remains constant):

$$\frac{\partial y}{\partial t} = f(t, y(t))$$

$$y(0) = y_0$$

where f is Lipschitz continuous with a Lipschitz constant L_f.

Using the following discretisation:

$$t_0 = 0; \quad t_{j+1} = t_j + \tau, \quad j = 1, 2, \ldots$$

$$y_0 = y(0);$$

Let τ be small enough to satisfy the following criterion:

$$\frac{3}{2} - \tau L_\mathrm{f} \geqslant \frac{1}{c}$$

where $c > 0$ is a constant.

The "Second Order Backward Euler" differentiation scheme takes the following form:

$$\begin{aligned}\frac{\partial y}{\partial t}(t_j) &\approx \frac{1}{\tau}\left(\frac{3}{2}y(t_j) - 2y(t_{j-1}) + \frac{1}{2}y(t_{j-2})\right) \\ &\approx f(t_j, y(t_j))\end{aligned} \tag{A.1}$$

The exact values $y(t_j)$ are approximated by the numerical values y_j;

So the algebraic equation to be solved is the following:

$$\frac{1}{\tau}\left(\frac{3}{2}y_j - 2y_{j-1} + \frac{1}{2}y_{j-2}\right) = f(t_j, y_j) \tag{A.2}$$

where y_{j-1} and y_{j-2} are known from the previous time steps and y_j is to be determined.

The local error (g_j) of this discretisation is the difference of the two sides of (A.1):

$$
\begin{aligned}
g_j := g(t_j,\tau) &= \frac{1}{\tau}\left(\frac{3}{2}y(t_j) - 2y(t_{j-1}) + \frac{1}{2}y(t_{j-2})\right) - f(t_j, y(t_j)) \\
&= \frac{1}{\tau}\left\{\frac{3}{2}y(t_j) - 2\left(y(t_j) - \tau\frac{\partial y}{\partial t}(t_j)\right.\right. \\
&\quad \left. + \frac{\tau^2}{2}\frac{\partial^2 y}{\partial t^2}(t_j) - \frac{\tau^3}{6}\frac{\partial^3 y}{\partial t^3}(t_j) + O(\tau^4)\right) \\
&\quad \left. + \frac{1}{2}\left(y(t_j) - 2\tau\frac{\partial y}{\partial t}(t_j) + \frac{4\tau^2}{2}\frac{\partial^2 y}{\partial t^2}(t_j) - \frac{8\tau^3}{6}\frac{\partial^3 y}{\partial t^3}(t_j) + O(\tau^4)\right)\right\} \\
&\quad - f(t_j, y(t_j)) \\
&= \frac{1}{\tau}\left\{\tau\frac{\partial y}{\partial t}(t_j) - \frac{\tau^3}{3}\frac{\partial^3 y}{\partial t^3}(t_j) + O(\tau^4)\right\} - f(t_j, y(t_j)) \\
&= -\frac{\tau^2}{3}\frac{\partial^3 y}{\partial t^3}(t_j) + O(\tau^3)
\end{aligned} \tag{A.3}
$$

subtracting (A.2) from (A.3) we obtain:

$$
\frac{1}{\tau}\left(\frac{3}{2}e_j - 2e_{j-1} + \frac{1}{2}e_{j-2}\right) = f(t_j, y(t_j)) - f(t_j, y_j) + g_j \tag{A.4}
$$

where

$$e_j = y(t_j) - y_j$$

With the notation

$$\phi_j = \frac{f(t_j, y(t_j)) - f(t_j, y_j)}{y(t_j) - y_j}$$

(A.4) transforms into

$$
\begin{aligned}
\frac{3}{2}e_j &= 2e_{j-1} - \frac{1}{2}e_{j-2} \\
&\quad + \tau\frac{f(t_j, y(t_j)) - f(t_j, y_j)}{y(t_j) - y_j}(y(t_j) - y_j) + \tau g_j \\
e_j\left(\frac{3}{2} - \tau\phi_j\right) &= 2e_{j-1} - \frac{1}{2}e_{j-2} + \tau g_j
\end{aligned} \tag{A.5}
$$

The following transformations

$$
\begin{aligned}
\frac{2}{\frac{3}{2} - \tau\phi_j} &= \frac{2}{\frac{3}{2}} + \tau\frac{2\phi_j}{\frac{3}{2}\left(\frac{3}{2} - \tau\phi_j\right)} = \frac{4}{3} + \frac{4\tau\phi_j}{3\left(\frac{3}{2} - \tau\phi_j\right)} \\
\frac{\frac{1}{2}}{\frac{3}{2} - \tau\phi_j} &= \frac{\frac{1}{2}}{\frac{3}{2}} + \tau\frac{\frac{1}{2}\phi_j}{\frac{3}{2}\left(\frac{3}{2} - \tau\phi_j\right)} = \frac{1}{3} + \frac{\tau\phi_j}{3\left(\frac{3}{2} - \tau\phi_j\right)}
\end{aligned}
$$

yield:

$$
\begin{aligned}
e_j &= \left(\frac{4}{3} + \frac{4\tau\phi_j}{3\left(\frac{3}{2} - \tau\phi_j\right)}\right)e_{j-1} - \left(\frac{1}{3} + \frac{\tau\phi_j}{3\left(\frac{3}{2} - \tau\phi_j\right)}\right)e_{j-2} \\
&\quad + \frac{\tau}{\frac{3}{2} - \tau\phi_j}g_j \\
e_j &= \frac{4}{3}e_{j-1} - \frac{1}{3}e_{j-2} + \frac{\tau}{\frac{3}{2} - \tau\phi_j}\left(\frac{4}{3}\phi_j e_{j-1} - \frac{1}{3}\phi_j e_{j-2} + g_j\right)
\end{aligned}
$$

The following notations are introduced:

$$
\varepsilon_j = \begin{pmatrix} e_{j-1} \\ e_j \end{pmatrix}; \quad A = \begin{pmatrix} 0 & 1 \\ -\frac{1}{3} & \frac{4}{3} \end{pmatrix};
$$

$$
B_j = \begin{pmatrix} 0 & 0 \\ -\frac{1}{3}\phi_j\frac{1}{\frac{3}{2} - \tau\phi_j} & \frac{4}{3}\phi_j\frac{1}{\frac{3}{2} - \tau\phi_j} \end{pmatrix}; \quad v_j = \begin{pmatrix} 0 \\ \frac{1}{\frac{3}{2} - \tau\phi_j}g_j \end{pmatrix}
$$

Then the equation in a matrix notation becomes:

$$\varepsilon_j = A\varepsilon_{j-1} + \tau B_j\varepsilon_{j-1} + \tau v_j \tag{A.6}$$

Let S be a matrix with which SAS^{-1} is the Jordan normal form of A:

$$
S = \begin{pmatrix} -\frac{1}{2} & \frac{3}{2} \\ -\frac{1}{2} & \frac{1}{2} \end{pmatrix}, \qquad SAS^{-1} = \begin{pmatrix} 1 & 0 \\ 0 & \frac{1}{3} \end{pmatrix} \Rightarrow \|SAS^{-1}\|_\infty = 1
$$

where $\|P\|_\infty := \max_i \sum_j |p_{ij}|$.

After multiplying both sides of (A.6) from the left side by S and with the $S^{-1}S = I$ we get:

$$S\varepsilon_j = SAS^{-1}S\varepsilon_{j-1} + \tau SB_jS^{-1}S\varepsilon_{j-1} + \tau Sv_j$$

With the usual inequalities for norms:

$$
\begin{aligned}
\|\varepsilon_j\|_S &\leqslant \|SAS^{-1}\|_\infty\|\varepsilon_{j-1}\|_S + \tau\|S\|_\infty\|B_j\|_\infty\|S^{-1}\|_\infty\|\varepsilon_{j-1}\|_S \\
&\quad + \tau\|S\|_\infty\|v_j\|_\infty \\
\|\varepsilon_j\|_S &\leqslant \|\varepsilon_{j-1}\|_S + \tau 2\|B_j\|_\infty 4\|\varepsilon_{j-1}\|_S + \tau 2\|v_j\|_\infty \\
\|\varepsilon_j\|_S &:= \|S\varepsilon_j\|_\infty \\
\|B_j\|_\infty &= |\phi_j|\left|\frac{1}{\frac{3}{2} - \tau\phi_j}\right|\left(\frac{1}{3} + \frac{4}{3}\right) \leqslant L_f\left|\frac{1}{\frac{3}{2} - \tau\phi_j}\right|\frac{5}{3} \leqslant \frac{5}{3}L_f\frac{1}{\frac{3}{2} - \tau L_f} \\
\|v_j\|_\infty &= \left|\frac{1}{\frac{3}{2} - \tau\phi_j}g_j\right| \leqslant \frac{1}{\frac{3}{2} - \tau L_f}g_j
\end{aligned}
$$

Hence:

$$\|\varepsilon_j\|_S \leqslant \|\varepsilon_{j-1}\|_S + 8\tau\frac{5}{3}L_f\frac{1}{\frac{3}{2} - \tau L_f}\|\varepsilon_{j-1}\|_S + 2\tau\frac{1}{\frac{3}{2} - \tau L_f}|g_j|$$

Since

$$
\begin{aligned}
&\frac{3}{2} - \tau L_f \geqslant \frac{1}{c} \\
&\|\varepsilon_j\|_S \leqslant \left(1 + \frac{40}{3}\tau L_f c\right)\|\varepsilon_{j-1}\|_S + 2\tau c|g_j| \\
&\qquad \leqslant \left(1 + \frac{40}{3}\tau L_f c\right)^j\|\varepsilon_0\|_S + 2\tau c\sum_{k=1}^{j}|g|_k\left(1 + \frac{40}{3}\tau L_f c\right)^{j-k} \\
&\qquad \leqslant \left(1 + \frac{40}{3}\tau L_f c\right)^j\left(\|\varepsilon_0\|_S + 2\tau c\sum_{k=1}^{j}|g|_k\right) \\
&\qquad \leqslant e^{\frac{40}{3}\tau_j L_f c}\left(\|\varepsilon_0\|_S + 2\tau c\sum_{k=1}^{j}|g|_k\right)
\end{aligned}
$$

$$
\begin{aligned}
&w := Sv \\
&\|v\|_S = \|w\|_\infty \leqslant \|S\|_\infty\|v\|_\infty = 2\|v\|_\infty \\
&\|v\|_\infty = \|S^{-1}w\|_\infty \leqslant \|S^{-1}\|_\infty\|w\|_\infty = 4\|w\|_\infty \\
&\frac{1}{4}\|v\|_\infty \leqslant \|v\|_S \leqslant 2\|v\|_\infty
\end{aligned}
$$

So:

$$\frac{1}{4}\|\varepsilon_j\|_\infty \leqslant \|\varepsilon_j\|_S \leqslant e^{\frac{40}{3}\tau j L_\Gamma c}\left(2\|\varepsilon_0\|_\infty + 2\tau c\sum_{k=1}^{j}|g|_k\right)$$

$$\|\varepsilon_j\|_\infty \leqslant 8e^{\frac{40}{3}\tau j L_\Gamma c}\left(\|\varepsilon_0\|_\infty + \tau c\sum_{k=1}^{j}|g|_k\right)$$

Where

$$\|\varepsilon_j\| = \max(|e_{j-1}|;|e_j|) \Rightarrow |e_j| \leqslant \|\varepsilon_j\|_\infty$$

Let us assume that the initial values are correct and the initial error $\|\varepsilon_0\|_\infty$ is zero, so:

$$|e_j| \leqslant 8e^{\frac{40}{3}\tau j L_\Gamma c}\left(\tau c\sum_{k=1}^{j}|g_k|\right)$$

From (A.3):

$$g_j = -\frac{\tau^2}{3}\frac{\partial^3 y}{\partial t^3}(t_j) + O(\tau^3) \Rightarrow |g_j| \leqslant \frac{\tau^2}{3}\max\left|\frac{\partial^3 y}{\partial t^3}\right| + O(\tau^3)$$

So if $T = N\tau$, at the end of the simulation the global error will be:

$$|e_N| \leqslant 8e^{\frac{40}{3}TL_\Gamma c}\tau cN\left(\frac{\tau^2}{3}\max\left|\frac{\partial^3 y}{\partial t^3}\right| + O(\tau^3)\right)$$

$$= 8e^{\frac{40}{3}TL_\Gamma c}Tc\frac{\tau^2}{3}\max\left|\frac{\partial^3 y}{\partial t^3}\right| + O(\tau^3)$$

$$|e_N| \leqslant conste^{T}T\tau^2\max\left|\frac{\partial^3 y}{\partial t^3}\right| + O(\tau^3)$$

where *const* is a constant, independently of the time step.

If we assume that the flow velocity at a fixed spatial point is a harmonic function of time, $A\sin(ft)$, the maximum of the absolute value of the third derivative can be approximated with Af^3. The global error of the simulation after the last time step can be estimated as:

$$|e_N| \leqslant conste^{T}T\tau^2 Af^3 + O(\tau^3) \tag{A.7}$$

For our reference case, $Re = 200$ a certain optimum time step was determined. Our task is to keep the same error at other Reynolds numbers either.

The frequency of oscillation is proportional with the mean exit velocity (v) of the jet in each stage. The duration of both the transient and the quasi-steady parts of the simulation is inversely proportional with the frequency (to keep the relative frequency resolution of the spectrum constant) and thus with v.

The amplitude A of the velocity oscillation is also proportional with the mean velocity v (see explanation to Fig. 13). Finally, the exponential factor can be ignored since then we are on the conservative side. This factor decreases anyway with increasing velocity and tends to 1. Putting all the information together, the error is kept constant if τ is decreased according to

$$\tau \propto v^{-\frac{3}{2}} \tag{A.8}$$

So the time step has to be decreased stronger than inversely proportionally with the velocity to keep the error constant.

Appendix B. Supplementary data

Supplementary data associated with this article can be found, in the online version, at doi:10.1016/j.ijheatfluidflow.2007.04.011.

References

Bamberger, A., Baensch, E., Siebert, K., 2004. Experimental and numerical investigation of edge tones. Z. Angew. Math. 84 (6), 1–15.

Brown, G.B., 1937. The vortex motion causing edge tones. Proc. Phys. Soc. Lond. 49, 493–507.

Crighton, D., 1992. The edgetone feedback cycle. Linear theory for the operating stages. J. Fluid Mech. 234, 361–391.

Curle, N., 1953. The mechanics of edge tones. Proc. Roy. Soc. A. 216, 412–424.

Holger, D., Wilson, T., Beavers, G., 1977. Fluid mechanics of the edgetone. J. Acoust. Soc. Am. 62, 1116–1128.

Howe, M.S., 1975. Contributions to the theory of aerodynamic sound, with application to excess jet noise and the theory of the flute. J. Fluid Mech. 71, 625–673.

Jones, A.T., 1942. Edge tones. J. Acoust. Soc. Am. 14, 131–139.

Kaykayoglu, R., Rockwell, D., 1986a. Unstable jet–edge interaction. Part 1. Instantaneous pressure fields at a single frequency. J. Fluid Mech. 169, 125–149.

Kaykayoglu, R., Rockwell, D., 1986b. Unstable jet–edge interaction. Part 2. Multiple frequency pressure fields. J. Fluid Mech. 169, 151–172.

Krothapalli, A. Horne, C., 1984. AIAA paper 84-2296.

Mattingly, G.E., Criminale, W.O., 1971. Disturbance characteristics in a plane jet. Phys. Fluids 14 (11), 2258–2264.

Nyborg, W.L., Burkhard, M.D., Schilling, H.K., 1952. Acoustical characteristics of jet–edge and jet–edge–resonator systems. J. Acoust. Soc. Am. 24, 293–304.

Ohring, S., 1986. Calculations of self-excited impinging jet flow. J. Fluid Mech. 163, 69–88.

Powell, A., 1961. On the edge tone. J. Acoust. Soc. Am. 33, 395–409.

Rockwell, D., Naudascher, E., 1979. Self-sustained oscillations of impinging free shear layers. Ann. Rev. Fluid Mech. 11, 67–94.

Ségoufin, C., Fabre, B., de Lacombe, L., 2004. Experimental investigation of the flue channel geometry influence on edge tone oscillations. Acta Acustica united with Acusica 90, 966–975.

Stoyan, G., Takó, G., 1995. Numerical methods. ELTE, Typotex, Budapest (in Hungarian).